

Discontinuous Galerkin Solution of the Navier-Stokes Equations on Deformable Domains

Per-Olof Persson* and Jaime Peraire†

Massachusetts Institute of Technology, Cambridge, MA 02139, U.S.A.

Javier Bonet‡

University of Wales Swansea, Swansea SA2 8PP, U.K.

We describe a method for computing time-dependent solutions to the compressible Navier-Stokes equations on variable geometries. We introduce a continuous mapping between a fixed reference configuration and the time varying domain. By writing the Navier-Stokes equations as a conservation law for the independent variables in the reference configuration, the complexity introduced by variable geometry is reduced to solving a transformed conservation law in a fixed geometry. The spatial discretization is carried out using the Discontinuous Galerkin method on unstructured meshes of triangles, while the time integration is performed using an explicit Runge-Kutta method. For general domain changes, the standard scheme fails to preserve exactly the free-stream solution which leads to a significant accuracy degradation even for high order approximations. This situation is remedied by adding an additional equation for the time evolution of the transformation Jacobian to the original conservation law and correcting for the accumulated metric integration errors. A number of results are shown to illustrate the flexibility of the approach to handle high order approximations on complex geometries.

I. Introduction

There is a growing interest in high-order methods for fluid problems, largely because of their ability to produce highly accurate solutions with minimum numerical dispersion. The Discontinuous Galerkin (DG) method produces stable discretizations of the convective operator for any order discretization. Moreover, it can be used with unstructured meshes of simplices, which appears to be a requirement for real-world complex geometries. In this paper, we present a high order DG formulation for computing high order solutions to problems with variable geometries.

Time varying geometries appear in a number of practical applications such as rotor-stator flows, flapping flight or fluid-structure interactions. In such cases, it is necessary to properly account for the time variation of the solution domain if accurate solutions are to be obtained. For the Navier-Stokes equations, there has been a considerable effort in the development of Arbitrary Lagrangian Eulerian (ALE) methods to deal with these situations.¹⁻⁴ In all these references, the satisfaction of the so-called Geometric Conservation Law, first introduced in Ref. 5, turns out to be a requirement to obtain schemes which are both stable and accurate. We also note that in these papers only second (or at most third) order accuracy for space and time is demonstrated.⁶ A common feature to these efforts is that the discretization of the equations is carried out on a deforming grid and thus the metric changes over time.

An alternative approach is that presented in Ref. 7 using a high order finite difference approach. There, a time varying mapping is constructed between a fixed reference domain and the real time-varying domain geometry.⁸ The original conservation law is first transformed to the reference configuration and then solved using a high order compact difference scheme. In this method, the actual computation is carried out on a

*Instructor, Department of Mathematics, MIT, 77 Massachusetts Avenue 2-363A, Cambridge, MA 02139. E-mail: persson@mit.edu. AIAA Member.

†Professor, Department of Aeronautics and Astronautics, MIT, 77 Massachusetts Avenue 37-451, Cambridge, MA 02139. E-mail: peraire@mit.edu. AIAA Associate Fellow.

‡Professor, School of Engineering, University of Wales Swansea, Swansea SA2 8PP, U.K. E-mail: j.bonet@swansea.ac.uk.

fixed mesh and the variable domain geometry is accounted for through a modification of the fluxes in the conservation law. This approach is simple and allows for arbitrarily high order solutions to be obtained. Unfortunately, the satisfaction of the Geometric Conservation Law is not guaranteed for general grid motions and correction terms are required to ensure preservation of constant solutions. One of the disadvantages of the correction terms proposed in Ref. 7 is that they are non-conservative and therefore their use for solutions involving strong shocks is unclear.

In this paper, we follow a similar approach to that presented in Ref. 7. That is, the equations are always discretized on a fixed reference domain. The spatial discretization is carried out using the Discontinuous Galerkin method on a mesh of triangles, and the time integration is done with an explicit Runge-Kutta scheme. In order to ensure that constant solutions in the physical domain are preserved exactly, we introduce an additional scalar equation in which the Jacobian of the transformation is integrated numerically using the same spatial and time discretization schemes. This numerically integrated Jacobian is used to correct for integration errors in the conservation equations. It turns out that for continuous mappings, this additional equation can be integrated locally within each element. Therefore, it can be segregated from the global system and dealt with separately, thus incurring a very small computational overhead. Several examples are presented and high orders of convergence are shown. Here, we consider polynomial approximations up to $p = 5$ and fourth order time integration. Although the method presented can be used in 3D without changes, in this paper, we only consider 2D examples. For the examples considered the mapping is given explicitly in terms of the boundary motion. We use blending functions to propagate the boundary movement into the domain. In most cases, the motion of the domain is prescribed beforehand, but we also show some examples involving simple 2D aero-elastic sections in which the airfoil pitch angle, and hence the geometry, is part of the solution.

II. ALE Formulation

When simulating problems involving time varying domains, the motion of the mesh must be accounted for in the solution process. We use an Arbitrary Lagrangian Eulerian (ALE) formulation, which allows us to move and deform the domains while preserving the high order accuracy. An important ingredient for our formulation is a time dependent mapping between a fixed reference domain and the physical deformable domain.

A. The Mapping

Let the physical domain of interest be denoted by $v(t)$ and the fixed reference configuration be denoted by V (see figure 1). Let $\mathcal{G}(\mathbf{X}, t)$ denote a one-to-one time dependent mapping between V and $v(t)$. Thus a point \mathbf{X} in V , is mapped to a point $\mathbf{x}(t)$ in $v(t)$, which is given by $\mathbf{x} = \mathcal{G}(\mathbf{X}, t)$. In order to transform the Navier-Stokes equations from the physical (\mathbf{x}, t) domain to the reference (\mathbf{X}, t) domain, we require some differential properties of the mapping. To this end, we introduce the mapping deformation gradient \mathbf{G} and the mapping velocity \mathbf{v}_X as

$$\mathbf{G} = \nabla_{\mathbf{X}} \mathcal{G}, \quad \mathbf{v}_X = \left. \frac{\partial \mathcal{G}}{\partial t} \right|_{\mathbf{X}}. \quad (1)$$

In addition, we denote the Jacobian of the mapping by $g = \det(\mathbf{G})$. We note that corresponding infinitesimal vectors $d\mathbf{L}$ in V and $d\mathbf{l}$ in $v(t)$ are related by $d\mathbf{l} = \mathbf{G}d\mathbf{L}$. Also, the elemental volumes are related by $dv = g dV$. From this, we can derive an expression for the area change. Let $d\mathbf{A} = \mathbf{N}dA$ denote an area element which after deformation becomes $d\mathbf{a} = \mathbf{n}da$. Here, \mathbf{N} and \mathbf{n} are the unit normals in V and $v(t)$, respectively. We then have that, $dV = d\mathbf{L} \cdot d\mathbf{A}$ and $dv = d\mathbf{l} \cdot d\mathbf{a}$. Therefore, we must have that

$$\mathbf{n} da = g\mathbf{G}^{-T} \mathbf{N} dA, \quad \text{and} \quad \mathbf{N} dA = g^{-1} \mathbf{G}^T \mathbf{n} da. \quad (2)$$

B. Transformed Equations

The Navier-Stokes equations in the physical domain (\mathbf{x}, t) are written as a system of conservation laws

$$\left. \frac{\partial \mathbf{U}_x}{\partial t} \right|_{\mathbf{x}} + \nabla_{\mathbf{x}} \cdot \mathbf{F}_x(\mathbf{U}_x, \nabla_{\mathbf{x}} \mathbf{U}_x) = 0, \quad (3)$$

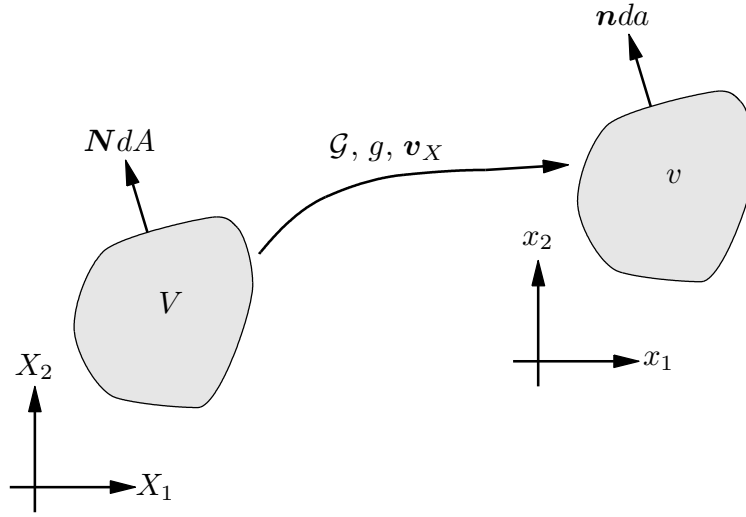


Figure 1. Mapping between the physical and the reference domains.

where \mathbf{U}_x is the vector of conserved variables and \mathbf{F}_x are the corresponding fluxes. Here, we write \mathbf{F}_x is a function of \mathbf{U}_x as well as $\nabla_x \mathbf{U}_x$ to indicate that the fluxes can indeed include viscous effects.

In order to obtain the corresponding conservation law written in the reference configuration we re-write the above equation in an integral form as

$$\int_{v(t)} \left. \frac{\partial \mathbf{U}_x}{\partial t} \right|_x dv + \int_{\partial v} \mathbf{F}_x \cdot \mathbf{n} da = \mathbf{0} \quad (4)$$

Note that the above expression follows directly from 3 by integrating over $v(t)$ and applying the divergence theorem. It is now possible to transform this integrals to the reference configuration. Consider first the second term:

$$\int_{\partial v} \mathbf{F}_x \cdot \mathbf{n} da = \int_{\partial V} \mathbf{F}_x \cdot (g \mathbf{G}^{-T} \mathbf{N}) dA = \int_{\partial V} (g \mathbf{G}^{-1} \mathbf{F}_x) \cdot \mathbf{N} dA \quad (5)$$

Similarly, the first integral is transformed by means of Reynolds transport theorem to give:

$$\int_{v(t)} \left. \frac{\partial \mathbf{U}_x}{\partial t} \right|_x dv = \frac{d}{dt} \int_{v(t)} \mathbf{U}_x dv - \int_{\partial v} (\mathbf{U}_x \mathbf{v}_X) \cdot \mathbf{n} da \quad (6)$$

$$= \frac{d}{dt} \int_V g^{-1} \mathbf{U}_x dV - \int_{\partial V} (\mathbf{U}_x \mathbf{v}_X) \cdot (g \mathbf{G}^{-T} \mathbf{N}) dA \quad (7)$$

$$= \int_V \left. \frac{\partial (g^{-1} \mathbf{U}_x)}{\partial t} \right|_X dV - \int_{\partial V} (g \mathbf{U}_x \mathbf{G}^{-1} \mathbf{v}_X) \cdot \mathbf{N} dA \quad (8)$$

using the divergence theorem once again enables an equivalent local conservation law in the reference domain to be derived as:

$$\left. \frac{\partial \mathbf{U}_X}{\partial t} \right|_X + \nabla_X \cdot \mathbf{F}_X(\mathbf{U}_X, \nabla_X \mathbf{U}_X) = 0, \quad (9)$$

where the transformed vector of conserved quantities and corresponding fluxes in the reference space are:

$$\mathbf{U}_X = g \mathbf{U}_x, \quad \mathbf{F}_X = g \mathbf{G}^{-1} \mathbf{F}_x - \mathbf{U}_X \mathbf{G}^{-1} \mathbf{v}_X, \quad (10)$$

and by simple chain rule,

$$\nabla_x \mathbf{U}_x = \nabla_X (g^{-1} \mathbf{U}_X) \mathbf{G}^{-T} = (g^{-1} \nabla_X \mathbf{U}_X - \mathbf{U}_X \nabla_X (g^{-1})) \mathbf{G}^{-T}. \quad (11)$$

III. Numerical Methods

In order to develop a DG method, we rewrite the above problem (9) as a system of first order equations

$$\frac{\partial \mathbf{U}_X}{\partial t} + \nabla_X \cdot \mathbf{F}_X(\mathbf{U}_X, \mathbf{Q}_X) = 0 \quad (12)$$

$$\mathbf{Q} - \nabla_X \mathbf{U}_X = 0 \quad (13)$$

Next, we introduce the ‘broken’ DG spaces \mathcal{V}^h and Σ^h associated with the triangulation $\mathcal{T}^h = \{K\}$ of V . In particular, \mathcal{V}^h and Σ^h denote the spaces of functions whose restriction to each element K are polynomials of order $p \geq 1$.

Following 9, we consider DG formulations of the form: find $\mathbf{U}_X^h \in \mathcal{V}^h$ and $\mathbf{Q}_X^h \in \Sigma^h$ such that for all $K \in \mathcal{T}^h$, we have

$$\int_K \frac{\partial \mathbf{U}_X^h}{\partial t} \mathbf{V} \, dV - \int_K \mathbf{F}_X(\mathbf{U}_X^h, \mathbf{Q}_X^h - X) \cdot \nabla_X \mathbf{V} \, dV - \int_{\partial K} \mathbf{V} (\hat{\mathbf{F}}_X \cdot \mathbf{N}) \, dA = 0 \quad \forall \mathbf{V} \in \mathcal{V}^h \quad (14)$$

$$\int_K \mathbf{Q}_X^h \mathbf{P} \, dV + \int_K \mathbf{U}_X^h \nabla_X \cdot \mathbf{V} \, dV - \int_{\partial K} \hat{\mathbf{U}}_X^h (\mathbf{P} \cdot \mathbf{N}) \, dA = 0 \quad \forall \mathbf{P} \in \Sigma^h \quad (15)$$

Here, the numerical fluxes $\hat{\mathbf{F}}_X \cdot \mathbf{N}$ and $\hat{\mathbf{U}}_X$ are approximations to $\mathbf{F}_X \cdot \mathbf{N}$ and to \mathbf{U}_X , respectively, on the boundary of the element K . The DG formulation is complete once we specify the numerical fluxes $\hat{\mathbf{F}}_X \cdot \mathbf{N}$ and $\hat{\mathbf{U}}_X$ in terms of (\mathbf{U}_X^h) and (\mathbf{Q}_X^h) and the boundary conditions. The flux term $\hat{\mathbf{F}}_X \cdot \mathbf{N}$ is decomposed into its inviscid and viscous parts:

$$\hat{\mathbf{F}}_X \cdot \mathbf{N} = \hat{\mathbf{F}}_N^{\text{inv}}(\mathbf{U}_X^h) + \hat{\mathbf{F}}_N^{\text{vis}}(\mathbf{U}_X^h, \mathbf{Q}_X^h) \quad (16)$$

The numerical fluxes $\hat{\mathbf{F}}_N^{\text{vis}}$ and $\hat{\mathbf{U}}_X$ are chosen according to the Compact Discontinuous Galerkin (CDG) method.¹⁰ This is a variant of the Local Discontinuous Galerkin (LDG) method⁹ but has the advantage of being compact on general unstructured meshes.

The inviscid numerical flux $\hat{\mathbf{F}}_N^{\text{inv}}(\mathbf{U}_X^h)$ is chosen according to the method proposed by Roe.¹¹ Note that this flux can be very easily derived from a standard eulerian Roe fluxes by noting that the flux \mathbf{F}_X given in 10 can be written as

$$\mathbf{F}_X = g \mathbf{G}^{-1} (\mathbf{F}_x - \mathbf{U}_x \mathbf{v}_X) ,$$

where $g \mathbf{G}^{-T} \mathbf{N}$ (from 2) is always continuous across the interface (assuming that \mathcal{G} is continuous), and the eigenvalues and eigenvectors of the Jacobian matrix for $\mathbf{F}_x - \mathbf{U}_x \mathbf{v}_X$ are trivially obtained from the Jacobian matrix for the standard eulerian flux \mathbf{F}_x .

Time integration is performed explicitly using a fourth order Runge-Kutta scheme. For the simulations coupled with simple structural models based on spring systems, the equations corresponding to the additional variables are integrated simultaneously with the DG system.

A. Geometric Conservation Law

It turns out that, for arbitrary mappings, a constant solution in the physical domain is not necessarily a solution of the discretized equations in the reference domain. Even though this error is typically very small for high order discretizations, the situation is quite severe for lower order approximations since the free-stream condition is not preserved identically. Satisfaction of the constant solution is often referred to as the Geometric Conservation Law (GCL) and is was originally discussed in 5. The source of the problem is the inexact integration of the Jacobian g of the transformation by the numerical scheme.

First, we note that using expressions 2, it is straightforward to prove the so-called Piola relationships, which hold for arbitrary vectors \mathbf{W} and \mathbf{w} :

$$\nabla_X \cdot \mathbf{W} = g \nabla_x \cdot (g^{-1} \mathbf{G} \mathbf{W}) , \quad \nabla_x \mathbf{w} = g^{-1} \nabla_X \cdot (g \mathbf{G}^{-1} \mathbf{w}) .$$

When the solution \mathbf{U}_x is constant, say $\bar{\mathbf{U}}_x$, we have

$$\nabla_X \cdot \mathbf{F}_X = g \nabla_x \cdot (\mathbf{F}_x - \bar{\mathbf{U}}_x \mathbf{v}_X) = -g \bar{\mathbf{U}}_x \nabla_x \cdot \mathbf{v}_X = -[\nabla_X \cdot (g \mathbf{G}^{-1} \mathbf{v}_X)] \bar{\mathbf{U}}_x .$$

Therefore, for a constant solution \bar{U}_x , equation 9 becomes

$$\left. \frac{\partial \mathbf{U}_X}{\partial t} \right|_X + \nabla_X \cdot \mathbf{F}_X = g^{-1} \bar{U}_x \left(\left. \frac{\partial g}{\partial t} \right|_X - \nabla_X \cdot (g \mathbf{G}^{-1} \mathbf{v}_X) \right).$$

We see that the right hand side is only zero if the equation for the time evolution for the transformation Jacobian g

$$\left. \frac{\partial g}{\partial t} \right|_X - \nabla_X \cdot (g \mathbf{G}^{-1} \mathbf{v}_X) = 0,$$

is integrated exactly by our numerical scheme. Since in general, this will not be the case, the constant solution \bar{U}_x in the physical space will not be preserved exactly.

An analogous problem was brought up in the formulation presented in 7. The solution proposed there was to add some corrections aimed at canceling the time integration errors. These terms are non-conservative and probably not suitable in the presence of strong shocks in the solutions. Here, we use a different approach. The system of conservation laws 9 is replaced by

$$\left. \frac{\partial (\bar{g} g^{-1} \mathbf{U}_X)}{\partial t} \right|_X - \nabla_X \cdot \mathbf{F}_X = 0 \quad (17)$$

where \bar{g} is obtained by solving the following equation using the same numerical scheme

$$\left. \frac{\partial \bar{g}}{\partial t} \right|_X - \nabla_X \cdot (g \mathbf{G}^{-1} \mathbf{v}_X) = 0. \quad (18)$$

We note that even though \bar{g} is an approximation to g , when the above equation is solved numerically its value will differ from that of g due to integration errors. It is straightforward to verify that 17 does indeed preserve a constant solution as desired. Finally, we point out that since the fluxes in equation 18 are continuous, the numerical flux is trivial to compute. Moreover, we note that equation 18 does not require information from neighboring elements and therefore can be solved on each element independently.

B. Mappings for Deformable Domains

In order to solve problems on moving domains, we need a procedure to define a mapping $\mathbf{x} = \mathcal{G}(\mathbf{X}, t)$ from the reference domain to the physical domain. One method that is commonly used in ALE simulations is to force the motion of the mesh nodes on the boundary and apply a mesh smoothing scheme to make reconstruct the mapping in the domain interior. Another technique is to solve additional equations (usually elliptic) for \mathbf{x} in the interior. For some of these algorithms, it may not be obvious to obtain accurate values for the mapping derivatives as required by our fluxes.

For the examples in this paper, we use a different approach which produces explicit expressions for the mappings. The procedure is illustrated in figure 2, where a mesh of an HT13 foil inside a circle is deformed in such a way that the foil is displaced and rotated but the circle is fixed. To do this, we use polynomial *blending functions* $r_n(x)$ of odd degree n , with $r(0) = 0$, $r(1) = 1$, and with $(n-1)/2$ vanishing derivatives at $x = 0$ and $x = 1$. For degree $n = 3$ this blending polynomial equals $r_3(x) = 3x^2 - 2x^3$, and for $n = 5$ it equals $r_5(x) = 10x^3 - 15x^4 + 6x^5$.

Next, we define a circle that contains the moving boundary, and compute the signed distance d_i from each mesh node \mathbf{X}_i to this circle. We choose a distance D from the circle such that all points at this distance are inside the domain, and compute a blending value for each mesh node:

$$b_i = \begin{cases} 0, & \text{if } d_i < 0 \\ 1, & \text{if } d_i > D \\ r(d_i/D), & \text{otherwise.} \end{cases} \quad (19)$$

Finally, we create a new set of mesh nodes \mathbf{Y} by deforming the entire mesh rigidly, according to the motion of the moving boundary, and compute our blended mesh nodes by

$$\mathbf{x}_i = b_i \mathbf{X}_i + (1 - b_i) \mathbf{Y}_i. \quad (20)$$

This approach has clearly some limitations, but for many cases it is remarkably simple and effective. It has the advantage that the mapping derivatives are easily obtainable since the mapping is given in explicit form. It is clearly that the regularity of the mapping must play an important role in the overall accuracy of the scheme. Here we use quintic $r_5(x)$ polynomials in all our simulations. We expect that in general continuous piecewise polynomially defined mappings will not degrade the accuracy, provided any discontinuities in the derivatives are concentrated at the element boundaries.

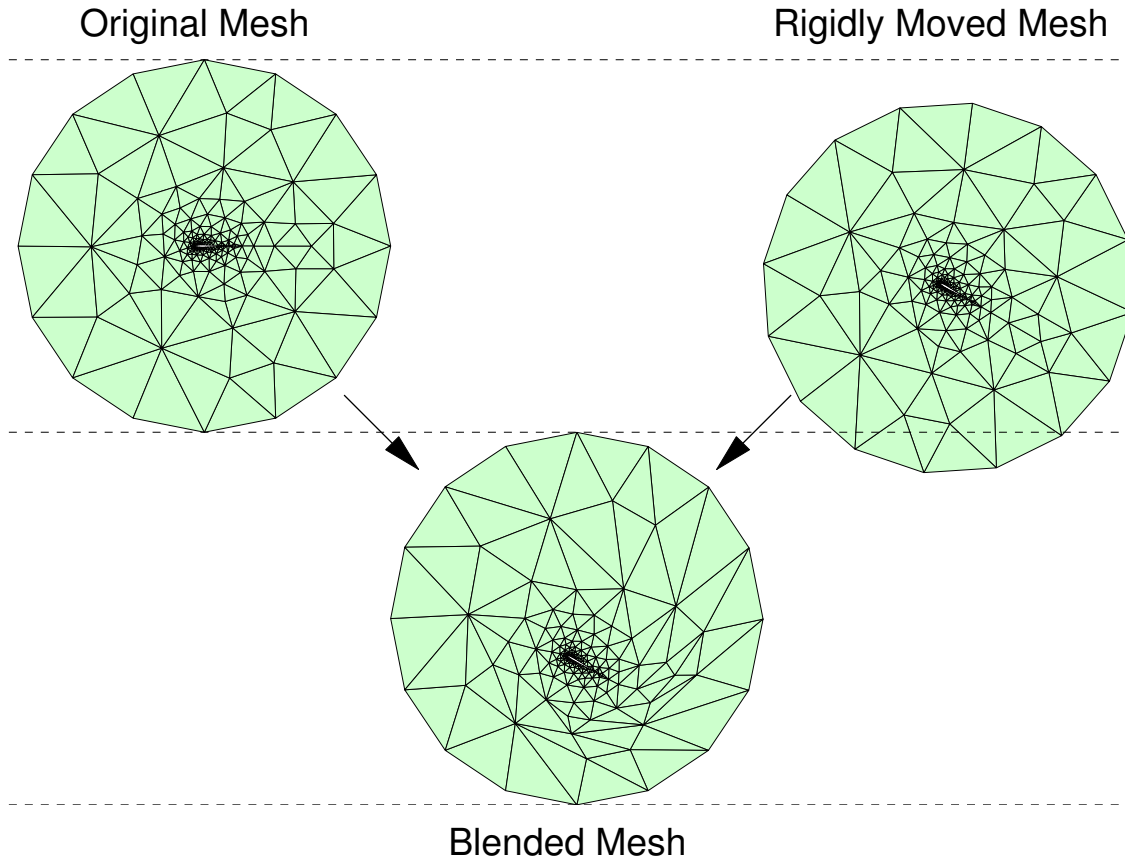


Figure 2. Deformation of a domain by blending of two rigid displacements.

IV. Results

A. Euler Vortex with Variable Mapping

To validate our solver and show that we retain the high-order accuracy after the domain mapping, we solve an inviscid model problem consisting of a compressible vortex in a rectangular domain.^{12,13} The vortex is initially centered at (x_0, y_0) and is moving with the free-stream at an angle θ with respect to the x -axis.

The analytic solution at (x, y, t) is given by

$$u = u_\infty \left(\cos \theta - \frac{\epsilon((y - y_0) - \bar{v}t)}{2\pi r_c} \exp\left(\frac{f(x, y, t)}{2}\right) \right) \quad (21)$$

$$v = u_\infty \left(\sin \theta + \frac{\epsilon((x - x_0) - \bar{u}t)}{2\pi r_c} \exp\left(\frac{f(x, y, t)}{2}\right) \right) \quad (22)$$

$$\rho = \rho_\infty \left(1 - \frac{\epsilon^2(\gamma - 1)M_\infty^2}{8\pi^2} \exp(f(x, y, t)) \right)^{\frac{1}{\gamma-1}} \quad (23)$$

$$p = p_\infty \left(1 - \frac{\epsilon^2(\gamma - 1)M_\infty^2}{8\pi^2} \exp(f(x, y, t)) \right)^{\frac{\gamma}{\gamma-1}} \quad (24)$$

where $f(x, y, t) = (1 - ((x - x_0) - \bar{u}t)^2 - ((y - y_0) - \bar{v}t)^2)/r_c^2$, M_∞ is the Mach number, $\gamma = c_p/c_v$, and $u_\infty, p_\infty, \rho_\infty$ are free-stream velocity, pressure, and density. The Cartesian components of the free-stream velocity are $\bar{u} = u_\infty \cos \theta$ and $\bar{v} = u_\infty \sin \theta$. The parameter ϵ measures the strength of the vortex and r_c is its size.

We use a domain of size 20-by-15, with the vortex initially centered at $(x_0, y_0) = (5, 5)$ with respect to the lower-left corner. The Mach number is $M_\infty = 0.5$, the angle $\theta = \arctan 1/2$, and the vortex has the parameters $\epsilon = 0.3$ and $r_c = 1.5$. We use periodic boundary conditions and integrate until time $t_0 = \sqrt{10^2 + 5^2}$, when the vortex has moved a relative distance of $(10, 5)$.

We solve the Euler equations on a regular rectangular mesh. The domain is mapped according to the following expressions:

$$x(\xi, \eta, t) = \xi + 2.0 \sin(2\pi\xi/20) \sin(\pi\eta/7.5) \sin(1.0 \cdot 2\pi t/t_0) \quad (25)$$

$$y(\xi, \eta, t) = \eta + 1.5 \sin(2\pi\xi/20) \sin(\pi\eta/7.5) \sin(2.0 \cdot 2\pi t/t_0) \quad (26)$$

We note that at times $t = 0$ and $t = t_0$, the mapping is the identity mapping which makes it straightforward to initialize and compare solutions. The solution and the deformed meshes at time $t = 0$ and $t = (3/8)t_0$ are shown in figure 3.

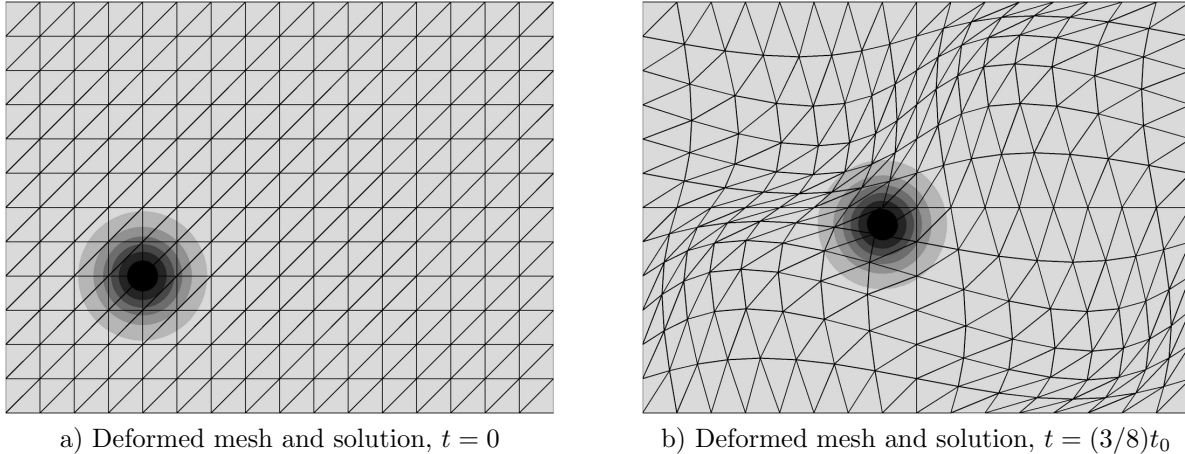


Figure 3. Meshes and solutions for initial conditions (a) and at time $t = (3/8)t_0$ (b). Note that the deformed mesh is used only for visualization, the calculations are done in the reference space using mapped equations.

We solve for a variety of mesh sizes and polynomial orders, and measure the error in the L_2 -norm. Figure 4 shows the convergence of the scheme, both with and without mapping of the domain. We note that we obtain optimal convergence $O(h^{p+1})$ in both cases, and that the mapped case has at most a factor of 8 larger error than the unmapped. The mapped scheme is of course expected to be less accurate, since this particular mapping is fairly extreme and generates large variations in the resolution of the vortex.

B. Free-stream Preservation

The above test has been performed with the modified scheme described above that ensures exact conservation of the free stream condition. To illustrate the effect of this modification, we solve using the same grid and

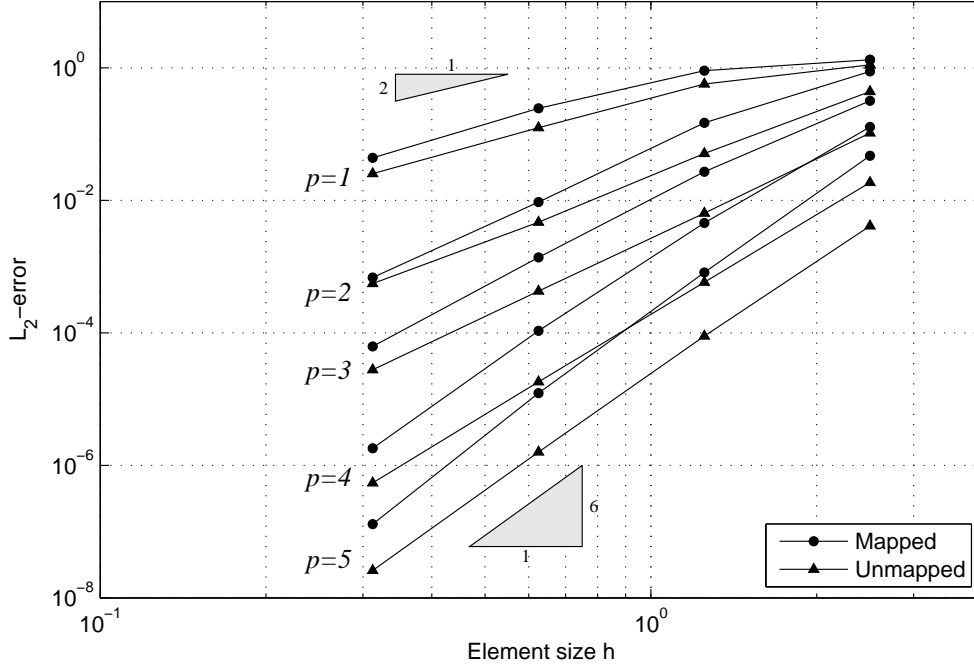


Figure 4. The convergence of the mapped and the unmapped schemes for the Euler vortex problem. Three mesh sizes are used and polynomial orders $p = 1$ to $p = 5$. The optimal convergence h^{p+1} is achieved in all the cases, although the constant is larger for the mapped cases because of the non-uniform resolution of the vortex.

time dependent mapping as in the previous example, but with uniform free-stream condition as the initial condition. We integrate in time until $t = 1.0$ with and without the correction (17),(18), and plot the L_2 -errors in figure 5.

Although the error without the correction converges to zero as $h \rightarrow 0$, we note that it can be quite large, especially if the solution is not well-resolved. With the correction the errors decrease by several orders of magnitude.

C. Flow around Oscillating Cylinder

In the next example, we consider two dimensional viscous flow around an oscillating cylinder of radius 1. The Reynolds number with respect to the diameter is 400 and the Mach number is 0.2. The y -displacement of the cylinder is given by

$$y_c(t) = A \sin(2\pi ft) \quad (27)$$

where $A = 4/3$ and $f = 0.1$. Our unstructured triangular mesh consists of 1316 elements and we use polynomials of degree $p = 4$ within each element.

We integrate for four periods (until $t = 40$) using two mappings – rigid vertical motion and a smooth blending between a displacement of the circle and a fixed mapping. The meshes and the solutions using the two techniques are shown in figure 6 at time $t = 17.5$, together with the time evolution of the lift and the drag coefficients. Although a numerical quantification of the error is hard because of the large sensitivity of the exact solution to small changes in the data, the results are very remarkably similar after a considerably large time integration interval.

D. Heaving and Pitching Foil in Wake

As an example of a more complex mapping, we solve for the flow around a NACA 0012 foil of length $c = 1$ placed in the wake of a D-section cylinder of diameter $d = 0.5$, following the experimental study in Ref. 14.

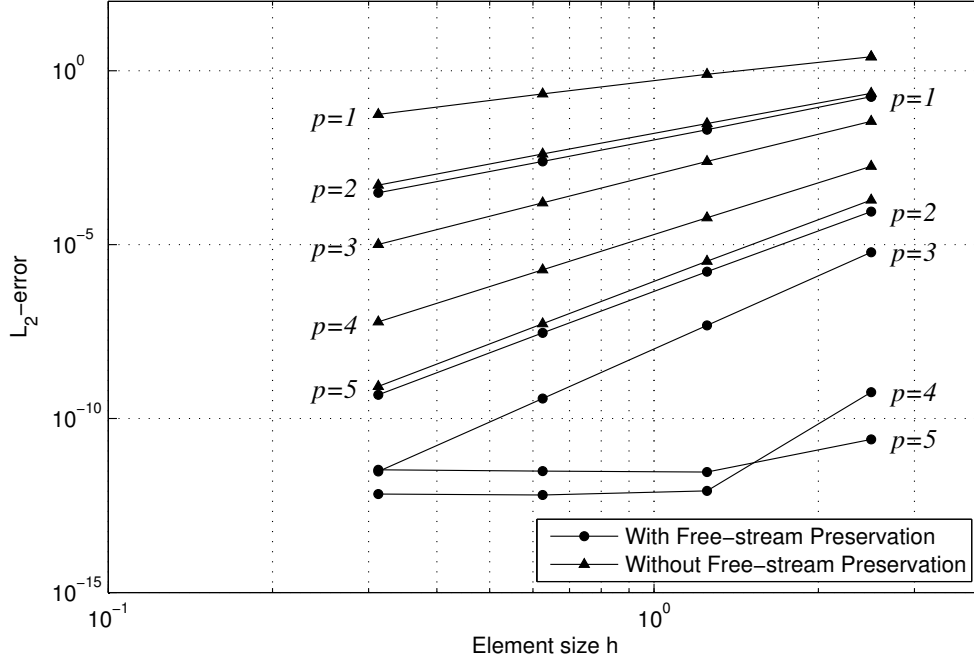


Figure 5. The convergence of a pure free-stream problem with and without the free-stream preservation technique.

Depending on the distance s between the center of the cylinder and the leading edge of the foil several modes of interaction can be identified. Here, we only present a preliminary computation for a particular value of $s = 4.25d = 2.125$ for illustration purposes. The cylinder and the foil oscillate in the vertical direction:

$$y(t) = A \sin(2\pi ft) \quad (28)$$

and the foil also rotates around the point $p = c/3$ from the leading edge:

$$\theta = a \sin(2\pi ft + \pi/2) \quad (29)$$

We choose the free-stream velocity $U = 1$ in the x -direction, the oscillation frequency $f = 0.2U/d = 0.4$, amplitudes $A = d/2 = 0.25$ and $a = \pi/6$. The flow has Mach number 0.2 and Reynolds number 550.

The mapping is a smooth blending of three meshes – the original mesh, a translation for the cylinder, and a translation and rotation for the foil. Figure 7 shows the reference mesh, a mapped mesh, Mach number and entropy plots, and time evolution of the lift and the drag on the two bodies.

E. Flow around Pitching Airfoil

In this test, we consider an aero-elastic section. We calculate the flow around a heaving/pitching HT13 airfoil. The motion of the airfoil in the vertical direction is a prescribed harmonic function,

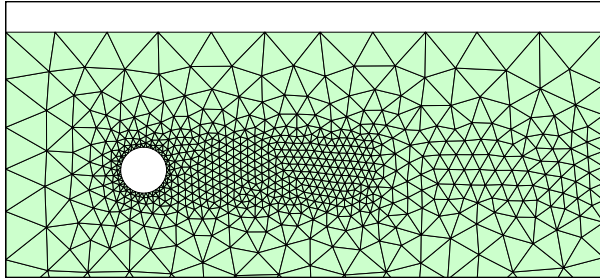
$$r_z(t) = h_0 \sin(\omega t). \quad (30)$$

The rotation of the airfoil is restrained by a torsional spring but otherwise the foil is free to rotate about the leading edge, see figure 8. This motion is determined by the angular momentum balance:

$$\ddot{\theta} + \omega_0^2 \theta = (M + S\ddot{r}_z)/I, \quad (31)$$

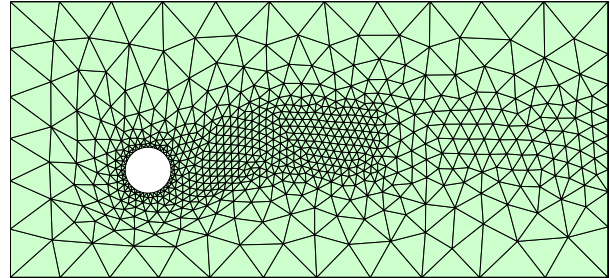
Here, we use the following non-dimensional values $\omega_0 = 1.5811$, $S = 10$, and $I = 3.333$, $\omega = 0.2$, airfoil chord equal to 1, and free stream velocity also equal to 1. In the above expression M , is the pitching moment on the foil about the leading edge. We write (31) as a system of first order equations and solve them together

Rigid Mapping

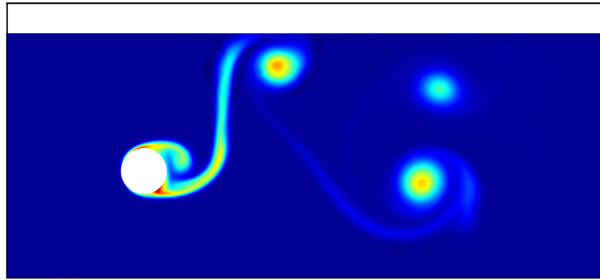


a) Mapped mesh (rigid)

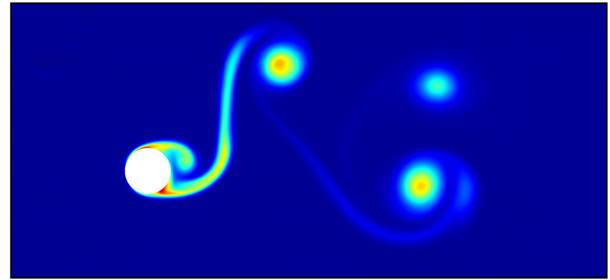
Blended Mapping



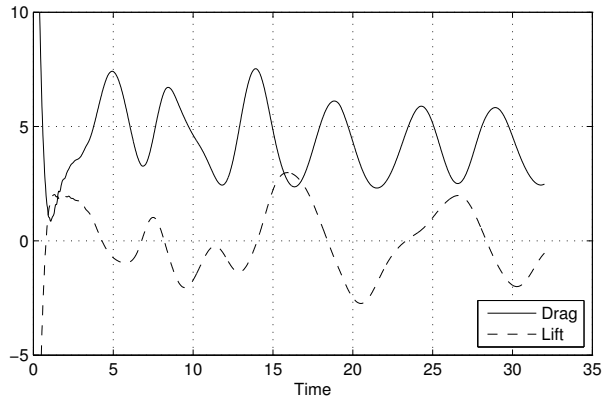
b) Mapped mesh (blended)



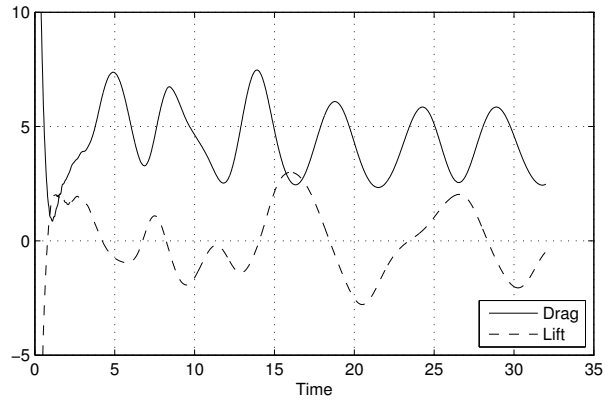
c) Entropy time $t = 17.5$ (rigid)



d) Entropy time $t = 17.5$ (blended)

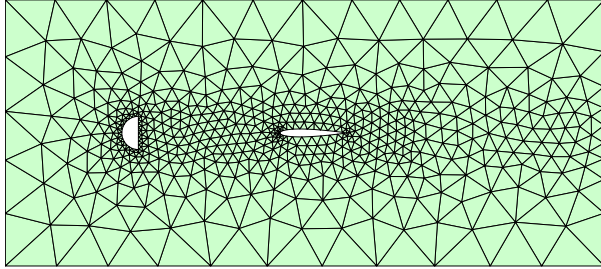


e) Time evolution, drag and lift (rigid)

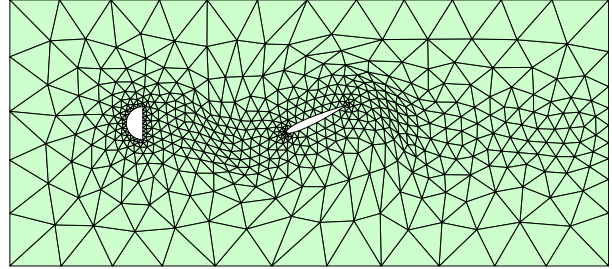


f) Time evolution, drag and lift (blended)

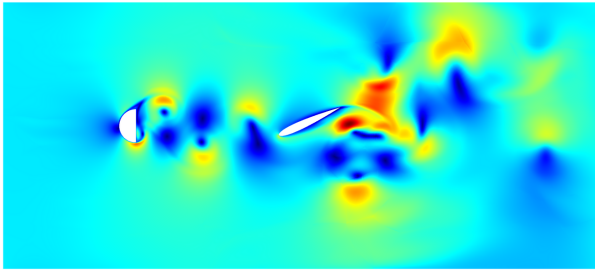
Figure 6. Meshes and plots of the entropies at time $t = 17.5$ for the the oscillating cylinder problem, and the time evolution of the lift and the drag coefficients.



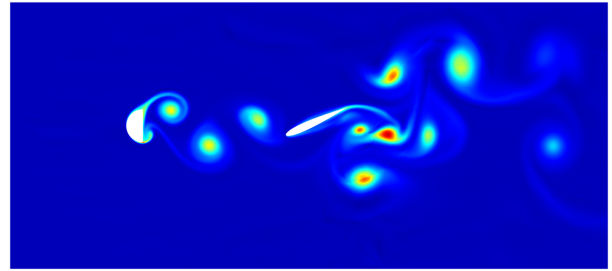
a) Reference domain and mesh



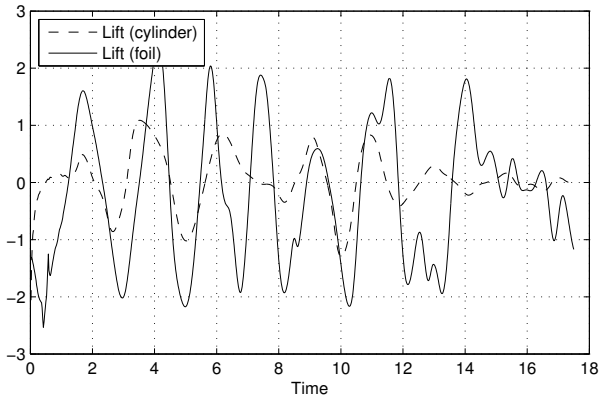
b) Mapped mesh (for visualization), time $t = 13.5$



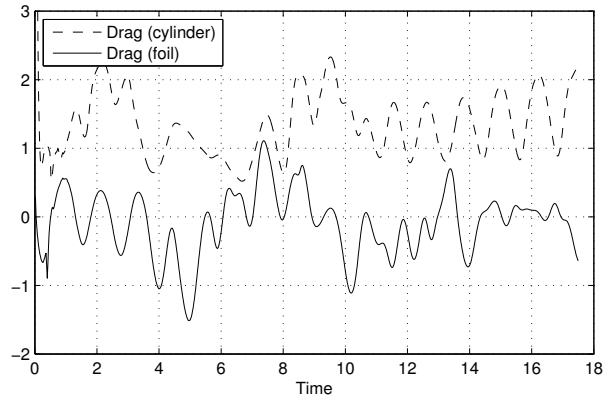
c) Mach number, time $t = 13.5$



d) Entropy, time $t = 13.5$



e) Time evolution, lift coefficient C_L



f) Time evolution, drag coefficient C_D

Figure 7. Two cylinders oscillating at equal amplitude and frequency, but with a phase difference.

with the fluid equations. Note that the two are coupled by M in (31), and by θ in the geometry definition for the fluid problem.

We use a relatively coarse mesh and calculate a $p = 3$ solution. The domain is mapped by a rigid motion, corresponding to a rotation around the origin and a displacement. Note that in this case since the mapping of the Jacobian g is always unity, the correction to ensure free-stream preservation is not required. In figure 9, time evolutions of the quantities r_z , θ , moment C_m , drag C_D , and lift C_L , are plotted for a typical set of parameters and two different amplitudes $h_0 = 0.75/4$ and $h_0 = 0.75$. The Reynolds number in this simulation is 5,000 and the Mach number is 0.2. We note that for the low amplitude case, the lift and the drag are fairly smooth functions of time during most of the period due to a fairly limited separation, while for the high amplitude case the flow separates at the leading edge and the evolution is less predictable. Note that both cases are highly non-linear and consequently well beyond the range of linear theory.

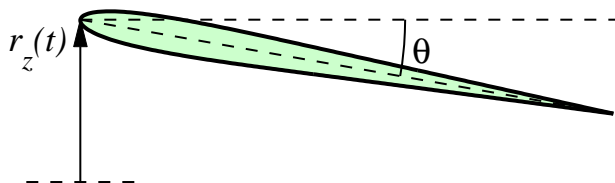


Figure 8. The pitching airfoil model.

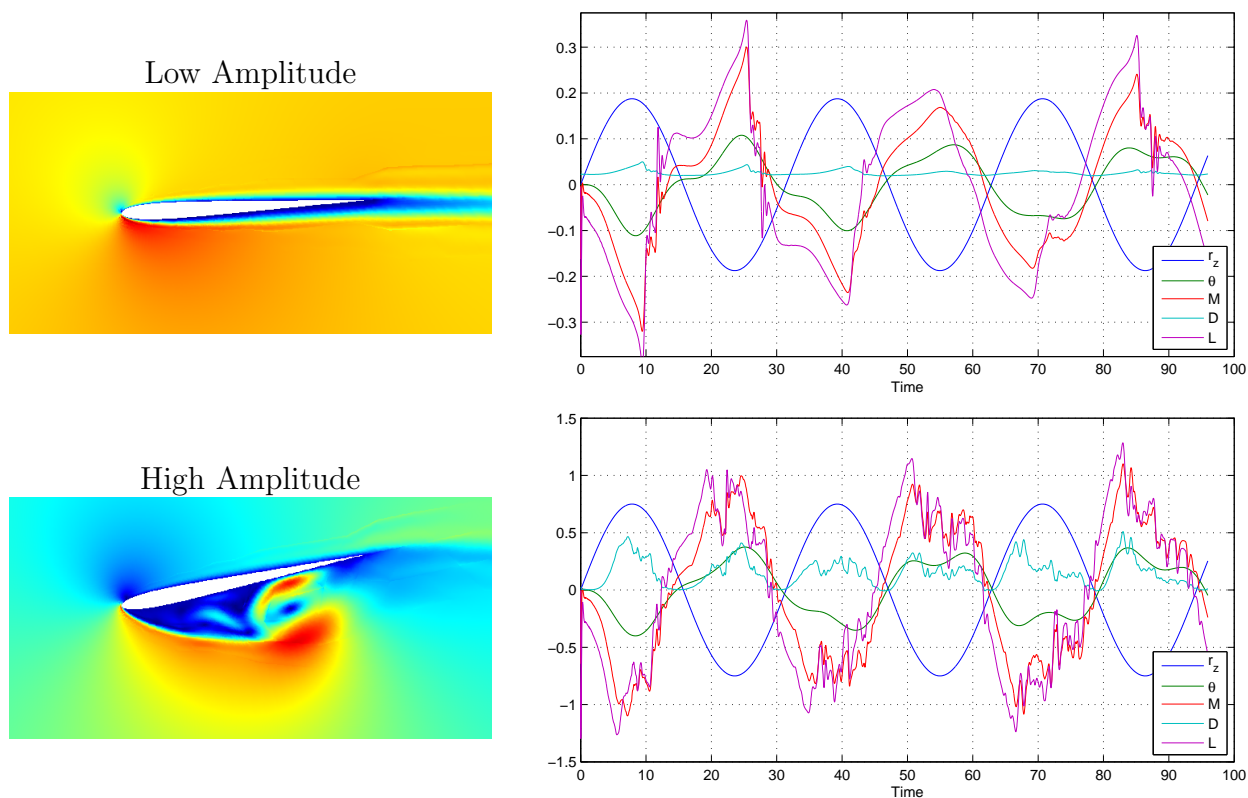


Figure 9. Time evolution of the pitching airfoil problem.

V. Acknowledgment

We would like to thank Mark Drela and David Willis for much valuable help with the pitching airfoil example. We would also like to acknowledge Anshul Mohnot for his help with the testing of the ALE

formulation. Finally, we would like to thank the Singapore-MIT Alliance for the partial support of this work.

References

- ¹Farhat, C. and Geuzaine, P., "Design and analysis of robust ALE time-integrators for the solution of unsteady flow problems on moving grids," *Comput. Methods Appl. Mech. Engrg.*, Vol. 193, No. 39-41, 2004, pp. 4073–4095.
- ²Venkatasubban, C. S., "A new finite element formulation for ALE (arbitrary Lagrangian Eulerian) compressible fluid mechanics," *Internat. J. Engrg. Sci.*, Vol. 33, No. 12, 1995, pp. 1743–1762.
- ³Lomtev, I., Kirby, R. M., and Karniadakis, G. E., "A discontinuous Galerkin ALE method for compressible viscous flows in moving domains," *J. Comput. Phys.*, Vol. 155, No. 1, 1999, pp. 128–159.
- ⁴Ahn, H. and Kallinderis, Y., "Strongly coupled flow/structure interactions with a geometrically conservative ALE scheme on general hybrid meshes," *Journal of Computational Physics*, to appear.
- ⁵Thomas, P. and Lombard, C., "Geometric conservation law and its application to flow computations on moving grids," *AIAA Journal*, Vol. 17, 1979.
- ⁶Formaggia, L. and Nobile, F., "Stability analysis of second-order time accurate schemes for ALE-FEM," *Comput. Methods Appl. Mech. Engrg.*, Vol. 193, No. 39-41, 2004, pp. 4097–4116.
- ⁷Visbal, M. R. and Gaitonde, D. V., "On the use of higher-order finite-difference schemes on curvilinear and deforming meshes," *J. Comput. Phys.*, Vol. 181, No. 1, 2002, pp. 155–185.
- ⁸Anderson, D., Tanehill, J., and Pletcher, R., *Computational Fluid Mechanics and Heat Transfer*, McGraw-Hill, New York, 1984.
- ⁹Cockburn, B. and Shu, C.-W., "The local discontinuous Galerkin method for time-dependent convection-diffusion systems," *SIAM J. Numer. Anal.*, Vol. 35, No. 6, 1998, pp. 2440–2463 (electronic).
- ¹⁰Peraire, J. and Persson, P.-O., "A Compact Discontinuous Galerkin (CDG) Method for Elliptic Problems," *submitted SIAM J. for Numerical Analysis*, 2006.
- ¹¹Roe, P. L., "Approximate Riemann solvers, parameter vectors, and difference schemes," *J. Comput. Phys.*, Vol. 43, No. 2, 1981, pp. 357–372.
- ¹²Erlebacher, G., Hussaini, M. Y., and Shu, C.-W., "Interaction of a shock with a longitudinal vortex," *J. Fluid Mech.*, Vol. 337, 1997, pp. 129–153.
- ¹³Mattsson, K., Svård, M., Carpenter, M., and Nordström, J., "High-Order Accurate Computations for Unsteady Aerodynamics," *Computers & Fluids*, Vol. 36, No. 3, 2007, pp. 636–649.
- ¹⁴Gopalkrishnan, R., Triantafyllou, M. S., Triantafyllou, G. S., and Barrett, D., "Active vorticity control in a shear flow using a flapping foil," *J. Fluid Mech.*, Vol. 274, 1994, pp. 1–21.
- ¹⁵Cockburn, B. and Shu, C.-W., "Runge-Kutta Discontinuous Galerkin Methods for Convection-Dominated Problems," *Journal of Scientific Computing*, Vol. 16, No. 3, 2001, pp. 173–261.